ACS Catalysis

RESEARCH ARTICLE

pubs.acs.org/acscatalysis

Iron-Catalyzed Olefin Epoxidation and cis-Dihydroxylation by Tetraalkylcyclam Complexes: the Importance of cis-Labile Sites

Yan Feng, Jason England, and Lawrence Que, Jr.*

Department of Chemistry and Center for Metals in Biocatalysis, University of Minnesota, Minneapolis, Minnesota 55455, United States

Supporting Information

ABSTRACT: [Fe(Me$_2$EBC)(OTf)$_2$], the iron(II) complex of the tetraazamacrocyclic Me$_2$EBC ligand (Me$_2$EBC = 4,11-dimethyl-1,4,8,11-tetraazabicyclo [6.6.2]hexadecane), has been investigated as a catalyst for olefin oxidation by H_2O_2 and compared to the closely related [Fe(TMC)(OTf)](OTf) complex (TMC = 1,4,8,11-tetramethyl-1,4,8,11-tetraazacyclotetradecane). Both complexes have tetraazamacrocyclic ligands based on cyclam that differ in how they coordinate to the iron center. This difference results in different orientations of their remaining coordination sites. Whereas the two sites on [Fe(Me$_2$EBC)(OTf)$_2$] are cis to each other, those of [Fe(TMC)(OTf)](OTf) are trans. Previous work on olefin oxidation by several nonheme iron catalysts has emphasized the importance of having two cis-labile sites to activate the H_2O_2 oxidant, particularly in effecting olefin cis-dihydroxylation, but there were differences in the ligand donor properties in the complexes studied. The fact that TMC and Me$_2$EBC provide essentially identical tertiary amine donors, but in different orientations, provides an excellent opportunity to assess the impact of ligand topology upon reactivity in the absence of other complicating factors. Indeed [Fe(Me$_2$EBC)(OTf)$_2$] was found to be an active catalyst with reactivity properties similar to those of the most thoroughly investigated iron catalyst [Fe(TPA)(OTf)$_2$] (TPA = tris(pyridin-2-ylmethyl)amine). In contrast, [Fe(TMC)(OTf)](OTf) only showed a limited ability for epoxidation and no facility for cis-dihydroxylation. This stark difference irrefutably demonstrates that cis-oriented labile sites are a fundamental requirement for successful nonheme iron catalyzed olefin oxidation. Additionally, mechanistic studies of [Fe(Me$_2$EBC)(OTf)$_2$] lead us to forward a similar Fe^{III}/Fe^{V} redox cycle as proposed for [Fe(TPA)(OTf)$_2$].

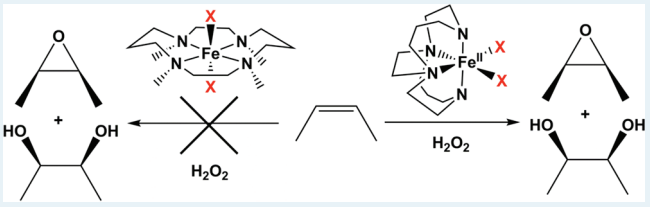

KEYWORDS: nonheme iron, olefin epoxidation, cis-dihydroxylation, cyclam

INTRODUCTION

The mononuclear nonheme oxygenase superfamily of enzymes has been found to be capable of catalyzing a startling array of chemical transformations, including epoxidation and cis-dihydroxylation of C=C bonds.[1,2] Of our particular interest in this regard are the Rieske dioxygenases, a class of enzymes that catalyze the cis-dihydroxylation of aromatic C=C bonds in the biodegradation of arenes.[3,4] The iron containing active sites of these Rieske dioxygenases[5] are supported by the "2-His-1-carboxylate facial triad" structural motif that characterizes the superfamily to which they belong, leaving up to three cis-labile sites for oxygen and/or substrate binding (Figure 1).[6,7] Reaction with dioxygen occurs upon 1e$^-$ reduction of the ferric resting of the enzyme, which is itself initiated by substrate binding within the active site domain. Subsequent injection of a second electron yields a $Fe^{III}(\eta^2\text{-}O_2)$ intermediate that in the case of naphthalene 1,2-dioxygenase (NDO) has been observed crystallographically.[8] Protonation activates the peroxo for reaction with the substrate, but it is a matter of some debate whether the putative $Fe^{III}(\eta^2\text{-}OOH)$ intermediate can carry out substrate cis-dihydroxylation directly, or must first undergo O−O bond heterolysis to form a HO-Fe^{V}=O active oxidant.[9−14]

Catalytic olefin cis-dihydroxylation is also an important chemical transformation in synthetic chemistry, where it is usually performed using the OsO_4-based "Sharpless Asymmetric Dihydroxylation".[15−18] This is a remarkably effective catalytic system, but concerns regarding the high toxicity and cost of osmium and the oxidants used has led to a search for alternatives.[19,20] In the past decade, our group and others have developed examples of first row transition metal catalysts for olefin cis-dihydroxylation.[21−28] Of particular note in this regard was a report by Che and co-workers detailing the use of an iron complex of a tetradentate macrocyclic ligand containing pyridine and tertiary amine donors to achieve high turnovers on a large reaction scale with oxone as the oxidant,[25] though the E factor (kg waste per kg product) is quite high.[19] Inspired by the Rieske dioxygenases, our own efforts have also focused upon the use of nonheme monoiron catalysts, but we prefer to use H_2O_2 as the terminal oxidant because of its low cost, low E factor, ease of handling, and the fact that its byproducts are environmentally benign.[29] Thus far, all effective iron catalysts contain either tetradentate or tridentate ligands, with at least two cis-oriented

Special Issue: Biocatalysis and Biomimetic Catalysis for Sustainability

Received: June 1, 2011
Revised: July 19, 2011
Published: July 26, 2011

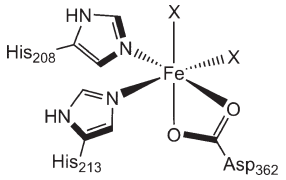

Figure 1. Naphthalene 1,2-dioxygenase (NDO) active site.

Chart 1. Ligand Structures

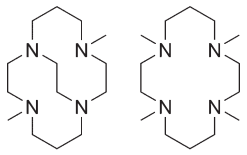

labile coordination sites. On this basis, cis-labile sites were proposed to be a key requirement for successful catalytic olefin dihydroxylation. However, major differences in the donor properties of the ligands used in these studies raise questions regarding the validity of this conclusion. In an effort to clarify this matter, we sought to compare the catalytic properties of the $Fe^{II}(OTf)_2$ complexes of Me_2EBC and TMC (Chart 1), two tetradentate ligands with near identical donor atoms that enforce different coordination geometries. TMC prefers to coordinate in an equatorial fashion and Me_2EBC coordinates facially, which results in a pair of trans-labile sites in the former case and cis-labile sites in the latter. The resulting systematic study of $[Fe^{II}(TMC)(OTf)](OTf)$ and $[Fe^{II}(Me_2EBC)(OTf)_2]$, and comparison with existing iron(II) catalysts, is rationalized on a mechanistic basis herein and provides unambiguous conclusions regarding the impact of labile site orientation upon the catalytic oxidation of olefins using hydrogen peroxide as the terminal oxidant.

EXPERIMENTAL SECTION

Materials and Synthesis. All reagents and anhydrous diethyl ether (Et_2O) were obtained from Sigma-Aldrich and used as received, unless otherwise noted. All olefin substrates were passed over basic alumina immediately prior to use. The solvents tetrahydrofuran (THF), dichloromethane (DCM), and acetonitrile (CH_3CN) were purified using a Vacuum Atmospheres Solvent Purifier and degassed prior to use. $H_2{}^{18}O_2$ (90% ^{18}O-enriched, 2 wt % solution in $H_2{}^{16}O$) and $H_2{}^{18}O$ (97% ^{18}O enriched) were purchased from Sigma-Aldrich and Shanghai Engineering Research Center of Stable Isotopes, respectively. $Fe(OTf)_2(CH_3CN)_2$, $[Fe(TMC)(OTf)](OTf)$, and $[Fe(Me_2EBC)Cl_2]$ were prepared according to literature procedures.[30−33]

Synthesis of [Fe(Me$_2$EBC)(OTf)$_2$]. A mixture of $[Fe(Me_2EBC)Cl_2]$ (265 mg, 0.7 mmol) and AgOTf (358 mg, 1.4 mmol) was stirred overnight in 5 mL of CH_2Cl_2. The AgCl precipitate formed during this time was removed by filtration, and the filtrate was reduced in volume and layered with Et_2O. The colorless crystals thereby obtained were isolated by filtration, washed with Et_2O, and dried under vacuum to give the product as a white solid (381 mg, 90%). Crystals of $[Fe(Me_2EBC)(OTf)_2]$ suitable for X-ray analysis were obtained by vapor diffusion of Et_2O into a concentrated CH_2Cl_2 solution of the complex. See Supporting Information for details regarding X-ray crystallographic analysis and Supporting Information, Table S1 for crystal data and structure refinement.

Characterization of [Fe(Me$_2$EBC)(OTf)$_2$]. ESI/MS: m/z 459 ($[Fe^{II}(Me_2EBC)(OTf)]^+$), 155 ($[Fe^{II}(Me_2EBC)]^{2+}$), both with the expected isotope distribution patterns (Supporting Information, Figure S1). Anal. Calcd. (found) for $C_{16}H_{30}F_6FeN_4O_6S_2$: C, 31.59 (31.56); H, 4.97 (5.14); N, 9.21 (9.16).

Instrumentation. NMR spectra were recorded on either a Varian Unity 300 or 500 MHz spectrometer at ambient temperature. Chemical shifts (ppm) were referenced to residual protic solvent peaks. High-resolution electrospray mass spectral (ESI-MS) experiments were performed on a Bruker (Billerica, MA) BioTOF II time-of-flight spectrometer, using a spray chamber voltage of 4000 V and a gas carrier temperature of 70 °C. Analysis of products from catalytic experiments were performed using a Perkin-Elmer AutoSystem gas chromatograph (AT-1701 column, 30 m) with a flame ionization detector. Gas chromatography/mass spectral analyses were performed on an HP 6890 GC (HP-5 MS column, 30 m) with an Agilent 5973 mass analyzer. A 4% NH_3/CH_4 mix was used as the ionization gas for chemical ionization analyses.

Reaction Conditions for Catalytic Oxidations. In a typical reaction, 10 equiv of H_2O_2 (diluted from 35% H_2O_2 solution with CH_3CN resulting in a 70 mM solution) was delivered by syringe pump under air over a period of 30 min at room temperature (20 °C) to a vigorously stirred CH_3CN solution containing iron complex and 1000 equiv of olefin substrate. The final concentrations were 0.7 mM iron complex, 7 mM H_2O_2, and 0.7 M olefin. The solution was stirred for an additional 5 min upon completion of H_2O_2 addition, after which organic products were esterified using 1 mL of acetic anhydride together with 0.1 mL of 1-methylimidazole. Subsequent to extraction using $CHCl_3$, an internal standard (naphthalene) was added, and the solution washed with 1 M H_2SO_4, sat. $NaHCO_3$, and H_2O. The organic layer was dried with $MgSO_4$ and subjected to GC analysis. The products were identified by comparison of their GC retention times with those of authentic compounds.

Substrate Limiting Reaction Conditions. In a typical reaction, H_2O_2 (diluted from 35% H_2O_2 solution with CH_3CN resulting in a 1 M solution) was delivered by syringe pump at a rate of 5 equiv (relative to iron) per minute at room temperature (20 °C) in air to a vigorously stirred CH_3CN solution containing iron complex, olefin substrate, and additive. The final concentration of iron complex was 0.7 mM. The solution was stirred for an additional 30 min after syringe pump addition, after which organic products were esterified using 1 mL of acetic anhydride together with 0.1 mL of 1-methylimidazole. Subsequent to extraction using $CHCl_3$, an internal standard (naphthalene) was added, and the solution was washed with 1 M H_2SO_4, sat. $NaHCO_3$, and H_2O. The organic layer was dried with $MgSO_4$ and subjected to GC analysis. The products were identified by comparison of their GC retention times with those of authentic compounds.

Isotope Labeling Studies. Conditions similar to those described above were used for isotope labeling studies, with the following exceptions. In experiments involving $H_2{}^{18}O$, 1000 equiv of $H_2{}^{18}O$ were added to the reaction solution prior to the injection of $H_2{}^{16}O_2$. In experiments involving $H_2{}^{18}O_2$, 10 equiv

of $H_2{}^{18}O_2$ (diluted by CH_3CN from the commercially available 2% $H_2{}^{18}O_2/H_2O$ solution, which contains 1:100 molar ratio of $H_2{}^{18}O$ to $H_2{}^{16}O$) was used instead of H_2O_2. The diol esterification procedure was the same as that detailed above. The data reported either represent a single reaction, or are the average of 2 reactions. The % ^{18}O values reported were calculated based on the ^{18}O-enrichment of the reagents containing the isotope.

RESULTS AND DISCUSSION

Structural Analysis. The crystal structure of $[Fe(Me_2EBC)(OTf)_2]$ is shown in Figure 2. It shows a C_2-symmetric six-coordinate iron center with the two triflate ligands occupying sites cis to each other. The Me_2EBC ligand adopts a cis-V stereochemistry associated with tetraalkylcyclam macrocycles because of the constraints imposed by the ethylene bridge that connects N1 and N1′,[34] much like the structures of $[Fe(Me_2EBC)Cl_2]$ and $[Mn(Me_2EBC)(OH)_2]^{2+}$ previously reported by Busch and co-workers.[33,35] In contrast, the structure of $[Fe(Me_2EBC)(OTf)_2]$ is clearly distinct from that of the related TMC complex $[Fe(TMC)(O_2SPh)](O_2SPh)$,[36] with the most obvious difference being the binding mode of the macrocyclic ligand to the metal center. Whereas the two remaining coordinating sites on $[Fe(Me_2EBC)(OTf)_2]$ are oriented cis relative to each other and occupied by the triflate anions, the two sites on $[Fe(TMC)(O_2SPh)](O_2SPh)$ are oriented trans to one another. However the latter complex is 5-coordinate, with only the site *syn* to the methyl groups being occupied by an ancillary ligand. Table 1 compares the bond lengths of $[Fe(Me_2EBC)(OTf)_2]$ with related complexes. $[Fe(Me_2EBC)(OTf)_2]$ exhibits nearly identical Fe−N bond lengths averaging 2.198 Å, while $[Fe(TMC)(O_2SPh)](O_2SPh)$ has Fe−N bond lengths ranging from 2.176(2) to 2.258(3) Å and averaging 2.215 Å.[36] All these distances are typical of high spin iron(II) complexes such as $[Fe(6\text{-}Me_3\text{-}TPA)(CH_3CN)]^{2+}$ (ave. Fe−N = 2.21 Å; 6-Me_3-TPA = tris((6-methylpyridin-2-yl) methyl)amine) and are much longer than those of low-spin $[Fe(TPA)(CH_3CN)_2]^{2+}$ (ave. Fe−N = 1.96 Å).[37]

NMR spectroscopy is a useful tool for assessing solution structure. Consistent with a $S = 2$ spin state, $[Fe^{II}(Me_2EBC)(OTf)_2]$ exhibits a ^1H NMR spectrum in CD_3CN solution consisting of a series of well-defined paramagnetically shifted and broadened resonances (Figure 3A). The number of peaks observed indicate that the C_2-symmetric solid-state structure of the complex is retained in solution. In contrast, the ^1H NMR spectrum of $[Fe^{II}(TMC)(OTf)](OTf)$ has a smaller number of resonances (Figure 3B) because of its C_{2v} symmetry. Notably, the CD_3CN solution ^{19}F NMR spectra of both complexes exhibit a single peak at −79.6 ppm (Figures 3C and D), which is associated with free triflate. In contrast, the ^{19}F NMR spectrum of $[Fe^{II}(Me_2EBC)(OTf)_2]$ in CD_2Cl_2 shows only one peak at 4.8 ppm, a chemical shift associated with bound triflate (Figure 3E), while the ^{19}F NMR spectrum of $[Fe^{II}(TMC)(OTf)](OTf)$ shows two peaks at 6.2 and −80.4 ppm, which are respectively associated with one free triflate and one coordinated triflate (Figure 3F). The ^{19}F NMR data in CD_3CN solution thus indicate that the triflate ligands are displaced by solvent molecules and that the catalyst precursors are in fact the dicationic complexes $[Fe^{II}(Me_2EBC)(CH_3CN)_2]^{2+}$ and $[Fe^{II}(TMC)(CH_3CN)]^{2+}$.

Catalytic Activities. Table 2 lists the catalytic activities of $[Fe(Me_2EBC)(OTf)_2]$ in the oxidation of various olefins with H_2O_2 as the oxidant. To allow direct comparison with published data, reactions were conducted using the conditions previously detailed for studies with $[Fe(TPA)(OTf)_2]$.[38] To simplify mechanistic studies and achieve high conversion of H_2O_2 into olefin oxidation product, a large excess of substrate was used and the H_2O_2 solution was introduced to the reaction system by syringe pump over a period of 30 min to avoid its disproportionation.

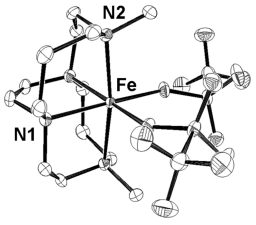

Figure 2. ORTEP plot of $[Fe(Me_2EBC)(OTf)_2]$ showing 50% probability thermal ellipsoids. Hydrogen atoms have been omitted for clarity.

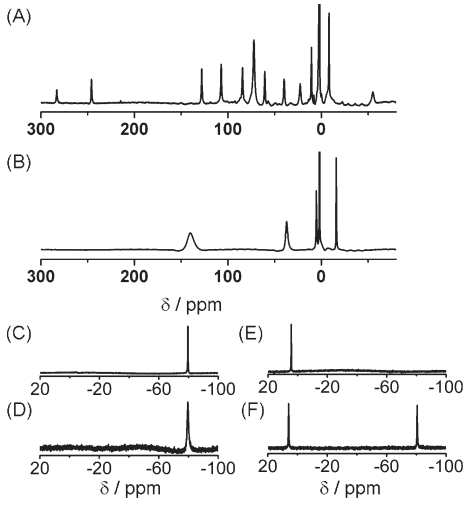

Figure 3. NMR spectra of $[Fe(Me_2EBC)(OTf)_2]$ and $[Fe(TMC)(OTf)](OTf)$. (A) ^1H NMR of $[Fe(Me_2EBC)(OTf)_2]$ in CD_3CN; (B) ^1H NMR of $[Fe(TMC)(OTf)_2]$ in CD_3CN; (C) ^{19}F-NMR of $[Fe(Me_2EBC)(OTf)_2]$ in CD_3CN; (D) ^{19}F-NMR of $[Fe(TMC)(OTf)](OTf)$ in CD_3CN; (E) ^{19}F-NMR of $[Fe(Me_2EBC)(OTf)_2]$ in CD_2Cl_2; (F) ^{19}F-NMR of $[Fe(TMC)(OTf)](OTf)$ in CD_2Cl_2.

Table 1. Bond Lengths (Å) Observed in Complexes Mentioned in This Work

	Fe−N1	Fe−N2	Fe−N3	Fe−N4	ref
$[Fe(Me_2EBC)(OTf)_2]$	2.197(1)	2.199(1)			this work
$[Fe(Me_2EBC)Cl_2]$	2.2574(13)	2.2634(13)	2.2866(14)	2.2748(13)	33
$[Fe(TMC)(O_2SPh)]^+$	2.231(3)	2.176(2)	2.258(3)	2.196(2)	36
$[Fe(TPA)(CH_3CN)_2]^{2+}$	1.99(1)	1.97(1)	1.92(1)	1.95(1)	37
$[Fe(6\text{-}Me_3\text{-}TPA)(CH_3CN)_2]^{2+}$	2.15(1)	2.25(1)	2.18(1)	2.24(1)	37

dx.doi.org/10.1021/cs200292h |ACS Catal. 2011, 1, 1035–1042

Table 2. Olefin Oxidation Catalyzed by $[Fe^{II}(Me_2EBC)(OTf)_2]$ and Related Complexes[a]

entry	ligand	olefin	epoxide [%RC][b]	*cis*-diol [%RC][b]	ref
1	Me_2EBC	*cis*-cyclooctene	1.8(1)	4.4(1)	this work
2	Me_2EBC	1-octene	0.3(1)	2.1(4)	this work
3	Me_2EBC	*cis*-2-heptene	1.1(1) [60]	4.1(1) [100]	this work
4	Me_2EBC	*t*-butyl acrylate	0.1(1)	0.9(3)	this work
5	Me_2EBC	dimethyl fumarate	0	0.4(1)	this work
6	TMC	*cis*-cyclooctene	1.0(1)	0	this work
7	TPA	*cis*-cyclooctene	3.4(1)	4.0(2)	38
8	6-Me_3-TPA	*cis*-cyclooctene	0.7(2)	4.9(6)	38
9	no complex	*cis*-cyclooctene	0	0	this work

[a] Reaction conditions: 10 equiv of H_2O_2 was added by syringe pump over a 30-min period (to minimize H_2O_2 disproportionation) at room temperature under air to a solution of 0.7 mM catalyst and 1000 equiv of substrate in CH_3CN. This solution was stirred for an additional 5 min before workup. See Experimental Section for further details. Yields expressed as turnover numbers, TON, (μmol product/μmol catalyst). [b] %RC, the percentage of retention of configuration of stereochemistry in the products of *cis*-2-heptene oxidation, expressed as $100 \times (A - B)/(A + B)$, where A = yield of *cis*-diol or *cis*-epoxide with retention of configuration and B = yield of epimer.

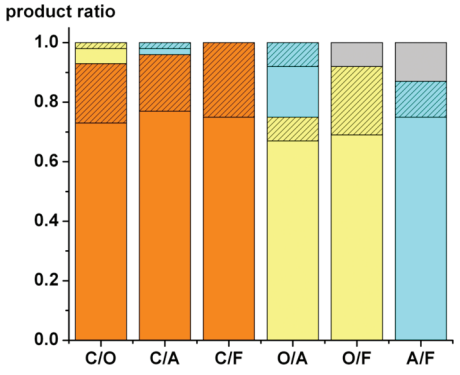

Figure 4. Competition oxidation results with equal amounts of two substrates catalyzed by $[Fe(Me_2EBC)(OTf)_2]$. C: *cis*-cyclooctene oxidation products in orange; O: 1-octene oxidation products in yellow; A: *t*-butyl acrylate oxidation products in cyan; F: dimethyl fumarate oxidation product in gray. Solid bars correspond to amount of *cis*-diol formed, while shaded bars correspond to amount of epoxide formed.

Table 2 shows that $[Fe(Me_2EBC)(OTf)_2]$ is a more effective catalyst for the oxidation of electron-rich olefins than for electron-poor ones (Table 2, entries 1−5). With cyclooctene as substrate, a 62% conversion of H_2O_2 into products was observed, with a diol-to-epoxide ratio of 2.4. With *cis*-2-heptene as substrate, a 52% conversion of H_2O_2 into products was achieved, with a diol-to-epoxide ratio of 3.7. In the case of 1-octene as substrate, the percentage conversion of H_2O_2 into products decreased to 24%, but the diol-to-epoxide ratio increased to 7. For the oxidation of electron-poor olefins, such as *t*-butyl acrylate and dimethyl fumarate, cis-dihydroxylation was strongly favored, but the yields of diol were low. *cis*-2-Heptene is a useful probe substrate because it can form cis- and/or trans-configured products, depending upon the reaction pathway followed. %RC is used to represent the percentage of retention of configuration in the products of oxidation, expressed as $100 \times (A - B)/(A + B)$, where A = yield of *cis*-diol or *cis*-epoxide with retention of configuration and B = yield of epimer. In our study, the oxidation of *cis*-2-heptene yielded the major *cis*-diol product with >99% retention of configuration, while the minor epoxide product showed a 60% retention of configuration. The observed high retention of configuration precludes *cis*-diol formation via epoxide ring-opening. Furthermore, a metal-based oxidant is strongly implicated for cis-dihydroxylation because a free radical oxidant like HO• is not known to form *cis*-diol products in the oxidation of olefins, nor would such large %RC values be expected.

Substrate competition studies provided further insight into the nature of the iron-based oxidant. Four substrates were selected for pairwise competition experiments, where equimolar amounts of two different substrates were oxidized under normal catalytic and workup conditions. As shown in Figure 4, the $[Fe(Me_2EBC)(OTf)_2]$ catalyst favored the oxidation of the more electron-rich olefin, with the order of oxidation preference found to be *cis*-cyclooctene >1-octene > *t*-butyl acrylate > dimethyl fumarate. Previously, our studies on iron-catalyzed olefin oxidation revealed that nonheme iron catalysts can be categorized into two classes.[39] Class A catalysts, such as $[Fe(TPA)(OTf)_2]$, preferentially oxidize electron-rich olefins and carry out both epoxidation and cis-dihydroxylation of olefins (Table 2, entry 7). On the other hand, Class B catalysts, exemplified by $[Fe(6\text{-}Me_3\text{-}TPA)(OTf)_2]$ (Table 2, entry 8), selectively perform olefin cis-dihydroxylation and oxidize electron-poor olefins like acrylate and fumarate more rapidly than electron-rich olefins. The oxidation preference observed for $[Fe(Me_2EBC)(OTf)_2]$ implicates the formation of an electrophilic oxidant, which indicates that it is a Class A catalyst.

Interestingly, the closely related $[Fe(TMC)(OTf)](OTf)$ complex is inactive as a catalyst for olefin oxidation. No cis-dihydroxylation of *cis*-cyclooctene was observed, and at best one turnover of the epoxide product was obtained (Table 2, entry 6). As $[Fe(Me_2EBC)(OTf)_2]$ and $[Fe(TMC)(OTf)](OTf)$ differ primarily in the orientation of the two potential labile sites at the iron center, the difference in their catalytic behavior supports the notion that two cis-labile sites are needed to promote this type of catalytic reactivity.

Catalytic Activities with Additives. In previous work, the catalytic behavior of $[Fe(TPA)(OTf)_2]$ and $[Fe(BPMEN)(OTf)_2]$ was found to be influenced by the presence of additives, with the addition of acetic acid resulting in increased turnover numbers and near exclusive formation of epoxide.[40−42] Similarly, the addition of 10 equiv of AcOH to $[Fe(Me_2EBC)(OTf)_2]$-catalyzed *cis*-cyclooctene oxidation reactions led to increased yields of products, with the overall conversion of H_2O_2 to

Table 3. Olefin Oxidation Catalyzed by [Fe(Me$_2$EBC)(OTf)$_2$] with Different Additives[a]

entry	additive	epoxide	*cis*-diol
1		1.8(1)	4.4(1)
2	0.5 AcOH	2.2	2.1
3	1 AcOH	3.8	1.7
4	10 AcOH	7.5	0.2
5	100 AcOH	7.6	0.1
6	1000 AcOH	7.3(1)	0
7	3000 AcOH	7.6	0
8	10 $ClCH_2COOH$	4.5	0.3
9	100 $ClCH_2COOH$	5.6	0
10	10 $Cl_2CHCOOH$	1.4	0.1
11	100 $Cl_2CHCOOH$	3.1	0
12	1 $HClO_4$	0.2	0.9
13	10 $HClO_4$	0.2(1)	0.3(1)
14	10 NaOAc	0.5(1)	0
15	10 2,6-lutidine	0.1	0.5
16[b]	1000 AcOH	0.3	0

[a] Reaction conditions: 10 equiv of H_2O_2 was added by syringe pump over a 30 min period (to minimize H_2O_2 disproportionation) at room temperature in air to a solution of catalyst (0.7 mM), 1000 equiv of *cis*-cyclooctene and additive in CH_3CN. This solution was stirred for an additional 5 min before workup. See Experimental Section for further details. Yields expressed as turnover numbers, TON, (μmol product/μmol catalyst). [b] Reaction catalyzed by [Fe(TMC)(OTf)](OTf).

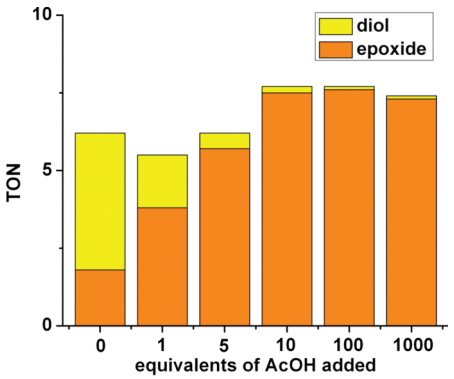

Figure 5. *cis*-Cyclooctene oxidation catalyzed by [Fe(Me$_2$EBC)(OTf)$_2$] with various equivalents of AcOH as additives. Reaction conditions are in Table 4 footnote a.

product rising from 62% to 75%, and a shift in the product distribution to favor almost exclusive formation of epoxide (Table 3, entry 4). On the other hand, the addition of 10 equiv of $HClO_4$ essentially killed the reaction, and even 1 equiv of $HClO_4$ was sufficient to inhibit catalysis significantly (Table 3, entry 12 and 13). These observations show that the role of acetic acid is not just to serve as a proton source. Catalytic activity was also almost completely lost with the addition of 10 equiv of NaOAc or 2,6-lutidine (Table 3, entries 14 and 15, respectively), which suggests that bases, whether coordinating or noncoordinating, are inimical to catalysis. The addition of 1000 equiv of HOAc to the [Fe(TMC)(OTf)](OTf)-catalyzed *cis*-cyclooctene oxidation reaction only served to decrease the yield of epoxide from 1 turnover to 0.3 (Table 3, entry 16).

In a more systematic study of the effect of acetic acid (Figure 5 and Table 3, entries 2−7), we found that even as little as 0.5 equiv of HOAc was sufficient to perturb the epoxide-to-diol ratio, and the maximum effect was attained with as little as 10 equiv. Carboxylic acids with lower pK_a (i.e., chloroacetic acid (pK_a = 2.9) and dichloroacetic acid (pK_a = 1.3)) were also effective at suppressing diol formation and shifting the product mixture to epoxide only, but the percentage conversion of H_2O_2 to product was lower than that for acetic acid (Table 3, entries 8 and 10). Adding more equivalents of chloroacetic acid and dichloroacetic acid increased conversion of H_2O_2 to epoxide (Table 3, entries 9 and 11). Taken together, these results can be rationalized by the existence of a binding equilibrium resulting from coordination of the added acid to the iron center, as postulated previously for [Fe(TPA)(OTf)$_2$], with the acid having the largest pK_a being a better ligand. The coordination of the carboxylic acid to the iron center promotes the epoxidation of *cis*-cyclooctene.

Given the positive effects of adding HOAc to the yield of epoxide, we explored more synthetically practical reaction conditions using 0.14 M *cis*-cyclooctene and 0.21 M H_2O_2, where substrate was the limiting reagent (Table 4). With 0.5 mol % [Fe(Me$_2$EBC)(OTf)$_2$] catalyst, 13% of substrate was converted into *cis*-diol (TON = 26) and 10% for epoxide (TON = 20). Upon addition of 0.7 M HOAc to the reaction mixture, the epoxide yield increased 5-fold to 62% (TON = 124), and the diol yield was suppressed to only 1%. While the overall yield of products in the absence of HOAc was lower for [Fe(Me$_2$EBC)(OTf)$_2$] than for [Fe(TPA)(OTf)$_2$] (69%), the overall yield improved significantly in the presence of 0.7 M HOAc for [Fe(Me$_2$EBC)(OTf)$_2$], while it dropped to 42% for [Fe(TPA)(OTf)$_2$].[41] On the other hand, comparisons with the epoxide-selective complex [Fe(BPMEN)(OTf)$_2$][41] showed that [Fe(Me$_2$EBC)(OTf)$_2$] was less effective as a catalyst, with or without adding AcOH. These results raise the possibility of developing practical applications of these complexes in synthetic chemistry.

Isotopic Labeling Studies. ^{18}O labeling experiments have proven useful in previous studies for deducing whether peroxide O−O bond cleavage occurs prior to the attack of substrate by establishing the source of the oxygen atoms incorporated into product.[24,38] As commercially available $H_2{}^{18}O_2$ usually comes as a 2 wt % solution in $H_2{}^{16}O$, the 10 equiv of $H_2{}^{18}O_2$ typically added in our labeling experiments was accompanied by 1000 equiv of $H_2{}^{16}O$. To corroborate these results, complementary labeling experiments with 10 equiv of $H_2{}^{16}O_2$ and 1000 equiv of $H_2{}^{18}O$ were also carried out. Previous experiments carried out for [Fe(TPA)(OTf)$_2$] and [Fe(6-Me$_3$-TPA)(OTf)$_2$] with *cis*-cyclooctene as substrate revealed two distinct labeling patterns.[38] For Class A catalyst [Fe(TPA)(OTf)$_2$], the *cis*-diol product incorporated one oxygen atom from H_2O_2 and the other from H_2O, results that led us to postulate a water-assisted mechanism for activating the peroxo O−O bond for cleavage. In contrast, for Class B catalyst [Fe(6-Me$_3$-TPA)(OTf)$_2$], both diol oxygens derived exclusively from H_2O_2, thereby requiring a nonwater-assisted pathway for H_2O_2 activation.

Analogous ^{18}O labeling experiments were carried out with [Fe(Me$_2$EBC)(OTf)$_2$]. Table 5 shows the percentage of ^{18}O incorporation into the epoxide and *cis*-diol products obtained from both $H_2{}^{18}O_2/H_2{}^{16}O$ and $H_2{}^{16}O_2/H_2{}^{18}O$ experiments. The [Fe(Me$_2$EBC)(OTf)$_2$]-catalyzed oxidation of *cis*-cyclooctene with $H_2{}^{18}O_2$ in the presence of 1000 equiv of $H_2{}^{16}O$ afforded epoxide with 82% incorporation of the ^{18}O label. When $H_2{}^{16}O_2$ was used in the presence of 1000 equiv of $H_2{}^{18}O$, 16% of

dx.doi.org/10.1021/cs200292h |ACS Catal. 2011, 1, 1035–1042

Table 4. *cis*-Cyclooctene Oxidation Catalyzed by Iron Complexes at 0.5 mol % Catalyst Loading[a]

					yield	
entry	complex	temp (°C)	additive	conversion	epoxide[d]	*cis*-diol[d]
1	$[Fe(Me_2EBC)(OTf)_2]$	20		44%	10%	13%
2	$[Fe(Me_2EBC)(OTf)_2]$	20	0.07 M HOAc	64%	55%	2%
3	$[Fe(Me_2EBC)(OTf)_2]$	20	0.7 M HOAc	77%	62%	1%
4[b]	$[Fe(Me_2EBC)(OTf)_2]$	20	0.7 M HOAc	52%	35%	1%
5	$[Fe(Me_2EBC)(OTf)_2]$	0		25%	5%	10%
6	$[Fe(Me_2EBC)(OTf)_2]$	0	0.7 M HOAc	77%	67%	1%
7[c]	$[Fe(TPA)(OTf)_2]$	0		n.r.	32%	37%
8[c]	$[Fe(TPA)(OTf)_2]$	0	0.7 M HOAc	n.r.	40%	2%
9[c]	$[Fe(BPMEN)(OTf)_2]$	0		n.r.	72%	3%
10[c]	$[Fe(BPMEN)(OTf)_2]$	0	0.7 M HOAc	n.r.	93%	1%

[a] Reaction conditions: H_2O_2 was added by syringe pump at a rate of 5 equiv/min (relative to catalyst, to minimize H_2O_2 disproportionation) in air to a CH_3CN solution of 0.7 mM catalyst, 0.14 M *cis*-cyclooctene. After syringe pump addition was completed, the reaction was stirred for another 30 min. [b] Oxidant is injected all at once. [c] Results from ref 41. Experiments were carried out at a catalyst concentration of 1 mM. [d] Yield is based on the substrate.

Table 5. Labeling Results of *cis*-Cyclooctene Oxidation Catalyzed by $[Fe(L)(OTf)_2]$

		epoxide		*cis*-diol		
		unlabeled	labeled	unlabeled	singly labeled	doubly labeled
Me_2EBC	$H_2{}^{18}O_2$ (2%)[a]	18%	82%	5%	88%	7%
Me_2EBC	1000 $H_2{}^{18}O$[b]	84%	16%	13%	86%	1%
TPA[c]	1000 $H_2{}^{18}O$[b]	90%	9%	14%	86%	
BPMEN[c]	1000 $H_2{}^{18}O$[b]	70%	30%	40%	60%	
^{Me2}PyTACN[d]	1000 $H_2{}^{18}O$[b]	35%	65%	12%	88%	

[a] Reaction conditions: 10 equiv of $H_2{}^{18}O_2$ was added by syringe pump over a 30 min period at room temperature in air to a solution of catalyst (0.7 mM) and 1000 equiv of *cis*-cyclooctene in CH_3CN. [b] Reaction conditions: 10 equiv of H_2O_2 was added by syringe pump over a 30 min period at room temperature in air to a solution of catalyst (0.7 mM), 1000 equiv of *cis*-cyclooctene and 1000 equiv of $H_2{}^{18}O$ in CH_3CN. [c] Results from ref 38. [d] Results from ref 43.

the epoxide was ^{18}O-labeled, a result complementary to the $H_2{}^{18}O_2$ experiment. Distinct from the epoxide labeling pattern, the *cis*-diol product showed dominant incorporation of one oxygen atom each from H_2O_2 and H_2O. Thus, all the oxygen present in both epoxide and diol products derived either from H_2O_2 or H_2O for epoxide and diol, with essentially no involvement of O_2 from air due to autoxidation.

Additional labeling experiments were carried out as a function of $H_2{}^{18}O$ concentration. As shown in Figure 6 and previously demonstrated for $[Fe(TPA)(OTf)_2]$,[38] the incorporation of ^{18}O from $H_2{}^{18}O$ into the epoxide and *cis*-diol products exhibits saturation behavior. This saturation behavior is reminiscent of Michaelis−Menten behavior in enzyme kinetics. It suggests the existence of a binding equilibrium of H_2O to the iron center before the rate determining O−O bond cleavage during the catalytic cycle, which is also illustrated by the linearity of the double reciprocal plot of the data (Figure 6, insets).

The incorporation of label from water incorporated into the oxidation products requires the participation of an oxidant that is able to undergo exchange with water in the course of the catalytic cycle. These labeling results are similar to those observed for *cis*-cyclooctene oxidation catalyzed by other $[Fe(L)(OTf)_2]$ complexes (L = TPA, BPMEN, and ^{Me2}PyTACN) (Table 5), but the extent of label incorporation from water into the epoxide product depends on the nature of tetradentate ligand. These variations are likely controlled by several factors: (a) the affinity of the iron center for the water ligand, (b) the rate of label exchange with the oxidant, and (c) the rate of reaction between the oxidant and the olefin. The labeling results for $[Fe(Me_2EBC)(OTf)_2]$ most closely resemble those of $[Fe(TPA)(OTf)_2]$.

Mechanistic Considerations. For $[Fe(TPA)(OTf)_2]$, the prototypical Class A catalyst, it is generally accepted that an Fe^{III}/Fe^{V} pair is involved in the catalytic cycle with an HO-Fe^{V}=O species as the active oxidant,[38] a notion supported by density functional theory (DFT) calculations.[44,45] This proposed mechanism is outlined in Scheme 1 and is based on the following observations: (1) the characterization of a low spin Fe^{III}−OOH complex in CH_3CN at −40 °C; (2) the incorporation of water into one atom of the *cis*-diol product in ^{18}O labeling experiments; and (3) the more rapid oxidation of more electron-rich olefins over electron-poor ones, implicating an electrophilic oxidant. This mechanism is distinct from that developing for Class B catalysts that involves an Fe^{II}/Fe^{IV} cycle with $Fe^{IV}(OH)_2$ as the active oxidant.[24]

The catalytic results with $[Fe(Me_2EBC)(OTf)_2]$ show a reactivity pattern very similar to that for $[Fe(TPA)(OTf)_2]$[38], thereby allowing classification of $[Fe(Me_2EBC)(OTf)_2]$ as a Class A catalyst. As implied in Scheme 1, the iron(II) catalyst must first be oxidized to iron(III) before the Fe^{III}−OOH intermediate can be formed and catalysis initiated. Such a lag phase was indeed observed for $[Fe^{II}(TPA)(OTf)_2]$, with the first 0.5 equiv of H_2O_2 added not producing any product.[38] Similarly, the addition

dx.doi.org/10.1021/cs200292h |ACS Catal. 2011, 1, 1035–1042

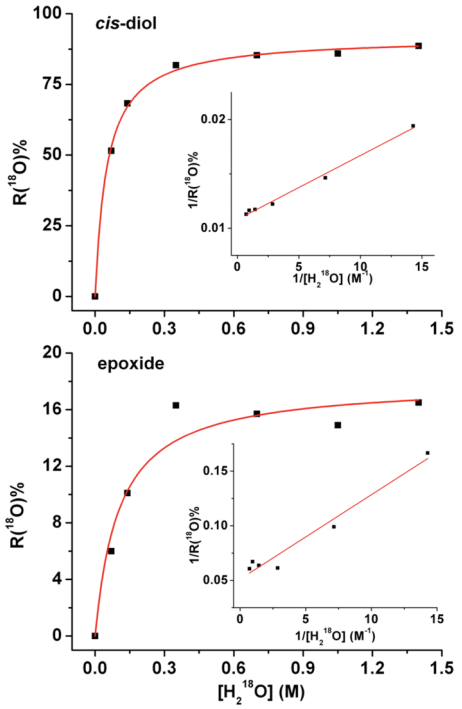

Figure 6. Percentage of ^{18}O-labeled epoxide and *cis*-diol product in the oxidation of *cis*-cyclooctene catalyzed by [Fe(Me$_2$EBC)(OTf)$_2$] with H_2O_2 as a function of the concentration of $H_2{}^{18}O$. Inset: double-reciprocal plot.

Scheme 1. Proposed Mechanism

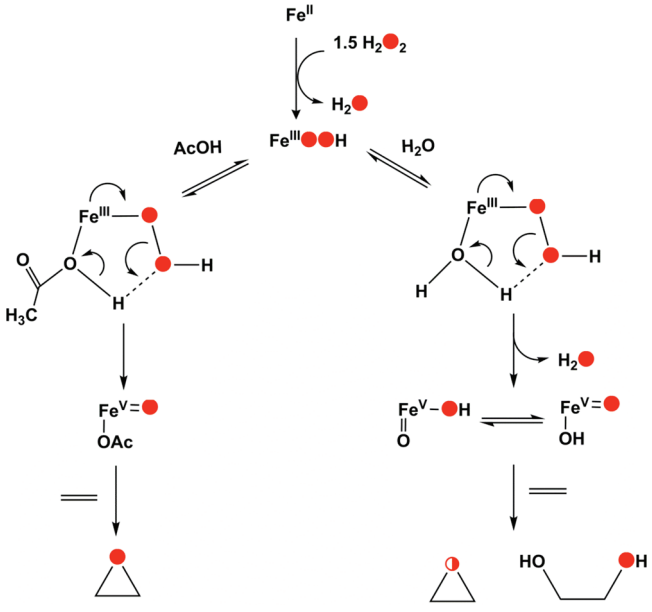

of 0.5 equiv of H_2O_2 to [Fe^{II}(Me$_2$EBC)(OTf)$_2$] afforded negligible quantities of product in both the absence and presence of added HOAc (Supporting Information, Table S3).

Labeling studies show that water is involved in the mechanism, and the observed saturation behavior in the extent of label incorporation from water suggests pre-equilibrium water binding to the metal center prior to O—O bond cleavage. Water is postulated to bind to a Fe^{III}—OOH center, which has yet to be observed for [Fe^{II}(Me$_2$EBC)(OTf)$_2$], to form a five-membered ring by hydrogen bonding to the terminal oxygen atom of the hydroperoxide (Scheme 1). This interaction is thought to promote heterolytic cleavage of the O—O bond to form an HO—Fe^{V}=O oxidant that is responsible for olefin epoxidation and cis-dihydroxylation, thereby rationalizing the ^{18}O labeling results that show water incorporation into both epoxide and *cis*-diol products. HOAc added in the reaction replaces the water ligand and serves as the proton donor that promotes O—O bond heterolysis. The resultant AcO—Fe^{V}=O oxidant is only capable of oxo transfer to the olefin substrate leading to exclusive epoxide formation.

Summary. Given the similarity of the donor atoms in the macrocyclic ligands of [Fe(TMC)(OTf)](OTf) and [Fe(Me$_2$EBC)(OTf)$_2$], it is remarkable that a simple change in the relative orientation of a pair of labile sites from trans to cis transforms an inactive complex into an effective catalyst for olefin oxidation. Furthermore, the positive effect of HOAc on product yield and epoxide selectivity for [Fe(Me$_2$EBC)(OTf)$_2$] catalysis, attributed to acetic acid binding to the iron center and its facilitation of O—O bond cleavage because of proton transfer to the distal oxygen atom of the Fe^{III}—OOH intermediate, is only possible for a complex with cis-labile sites. Indeed, not only does HOAc addition not exert an enhancing effect upon catalysis using [Fe(TMC)(OTf)](OTf), it is in fact inimical to its reactivity. A similar carboxylic-acid-derived enhancement in selectivity and yield has also been seen by White and co-workers in the catalytic functionalization of C—H bonds in the synthesis of complex organic molecules using a related nonheme iron complex containing a pair of cis-labile sites together with H_2O_2.[46,47] Lastly, the olefin cis-dihydroxylation facilitated by [Fe(Me$_2$EBC)(OTf)$_2$] has only ever been seen for complexes with cis-labile sites, from which it can be inferred that it is a fundamental prerequisite for such reactivity to be manifested. Considering the above points, it is not surprising, or perhaps even inevitable, that the "2-His-1-carboxylate facial triad", which contains three facially oriented nominally labile sites, is the prevailing structural motif found in the active sites of dioxygen activating mononuclear nonheme enzymes.

■ ASSOCIATED CONTENT

Supporting Information. Table S1 listing crystallographic data for [Fe(Me$_2$EBC) (OTf)$_2$], Tables S2 and S3 listing additional oxidation results, and Figure S1 showing the ESI-MS spectrum of [Fe(Me$_2$EBC)(OTf)$_2$]. This material is available free of charge via the Internet at http://pubs.acs.org.

■ AUTHOR INFORMATION

Corresponding Author

*E-mail: larryque@umn.edu.

Funding Sources

This work was supported by the United States Department of Energy (DE-FG02-03ER15455).

■ REFERENCES

(1) Costas, M.; Mehn, M. P.; Jensen, M. P.; Que, L., Jr. *Chem. Rev.* **2004**, *104*, 939–986.

(2) Abu-Omar, M. M.; Loaiza, A.; Hontzeas, N. *Chem. Rev.* **2005**, *105*, 2227–2252.
(3) *Microbial Degradation of Organic Compounds*; Gibson, D. T., Ed.; Marcel Dekker: New York, 1984.
(4) Gibson, D. T.; Parales, R. E. *Curr. Opin. Biotechnol.* **2000**, *11*, 236–243.
(5) Ferraro, D. J.; Gakhar, L.; Ramaswamy, S. *Biochem. Biophys. Res. Commun.* **2005**, *338*, 175–190.
(6) Hegg, E. L.; Que, L., Jr. *Eur. J. Biochem.* **1997**, *250*, 625–629.
(7) Koehntop, K. D.; Emerson, J. P.; Que, L., Jr. *J. Biol. Inorg. Chem.* **2005**, *10*, 87–93.
(8) Karlsson, A.; Parales, J. V.; Parales, R. E.; Gibson, D. T.; Eklund, H.; Ramaswamy, S. *Science* **2003**, *299*, 1039–1042.
(9) Wolfe, M. D.; Parales, J. V.; Gibson, D. T.; Lipscomb, J. D. *J. Biol. Chem.* **2001**, *276*, 1945–1953.
(10) Wolfe, M. D.; Lipscomb, J. D. *J. Biol. Chem.* **2003**, *278*, 829–835.
(11) Bassan, A.; Blomberg, M. R. A.; Siegbahn, P. E. M. *J. Biol. Inorg. Chem.* **2004**, *9*, 439–452.
(12) Neibergall, M. B.; Stubna, A.; Mekmouche, Y.; Munck, E.; Lipscomb, J. D. *Biochemistry* **2007**, *46*, 8004–8016.
(13) Chakrabarty, S.; Austin, R. N.; Deng, D.; Groves, J. T.; Lipscomb, J. D. *J. Am. Chem. Soc.* **2007**, *129*, 3514–3515.
(14) Ohta, T.; Chakrabarty, S.; Lipscomb, J. D.; Solomon, E. I. *J. Am. Chem. Soc.* **2008**, *130*, 1601–1610.
(15) Kolb, H. C.; VanNieuwenhze, M. S.; Sharpless, K. B. *Chem. Rev.* **1994**, *94*, 2483–2547.
(16) Johnson, R. A.; Sharpless, K. B. In *Catalytic Asymmetric Synthesis*, 2nd ed.; Ojima, I., Ed.; Wiley-VCH: New York, 2000; pp 357−398.
(17) Dupau, P.; Epple, R.; Thomas, A. A.; Fokin, V. V.; Sharpless, K. B. *Adv. Synth. Catal.* **2002**, *344*, 421–433.
(18) Zaitsev, A. B.; Adolfsson, H. *Synthesis* **2006**, *11*, 1725–1756.
(19) Sheldon, R. A. *Chem. Commun.* **2008**, 3352–3365.
(20) Beach, E. S.; Cui, Z.; Anastas, P. T. *Energy Environ. Sci.* **2009**, *2*, 1038–1049.
(21) Chen, K.; Que, L., Jr. *Angew. Chem., Int. Ed.* **1999**, *38*, 2227–2229.
(22) Bruijnincx, P. C. A.; Buurmans, I. L. C.; Gosiewska, S.; Moelands, M. A. H.; Lutz, M.; Spek, A. L.; Koten, G. v.; Klein Gebbink, R. J. M. *Chem.—Eur. J.* **2008**, *14*, 1228–1237.
(23) de Boer, J. W.; Browne, W. R.; Harutyunyan, S. R.; Bini, L.; Tiemersma-Wegman, T. D.; Alsters, P. L.; Hage, R.; Feringa, B. L. *Chem. Commun.* **2008**, 3747–3749.
(24) Oldenburg, P. D.; Feng, Y.; Pryjomska-Ray, I.; Ness, D.; Que, L. J. *J. Am. Chem. Soc.* **2010**, *132*, 17713–17723.
(25) Chow, T. W.; Wong, E. L.; Guo, Z.; Liu, Y.; Huang, J.; Che, C.-M. *J. Am. Chem. Soc.* **2010**, *132*, 13229–13230.
(26) Saisaha, P.; Pijper, D.; van Summeren, R. P.; Hoen, R.; Smit, C.; de Boer, J. W.; Hage, R.; Alsters, P. L.; Feringa, B. L.; Browne, W. R. *Org. Biomol. Chem.* **2010**, *8*, 4444–4450.
(27) de Boer, J. W.; Brinksma, J.; Browne, W. R.; Meetsma, A.; Alsters, P. L.; Hage, R.; Feringa, B. L. *J. Am. Chem. Soc.* **2005**, *127*, 7990–7991.
(28) de Boer, J. W.; Browne, W. R.; Brinksma, J.; Alsters, P. L.; Hage, R.; Feringa, B. L. *Inorg. Chem.* **2007**, *46*, 6353–6372.
(29) Tse, M. K.; Schroder, K.; Beller, M. In *Modern Oxidation Methods*, 2nd ed.; Bäckvall, J.-E., Ed.; Wiley-VCH: Weinheim, Germany, 2010; pp 1−36.
(30) Hagen, K. S. *Inorg. Chem.* **2000**, *39*, 5867–5869.
(31) Nam, W.; Ho, R. Y. N.; Valentine, J. S. *J. Am. Chem. Soc.* **1991**, *113*, 7052–7054.
(32) Weisman, G. R.; Rogers, M. E.; Wong, E. H.; Jasinski, J. P.; Paight, E. S. *J. Am. Chem. Soc.* **1990**, *112*, 8604–8605.
(33) Hubin, T. J.; McCormick, J. M.; Collinson, S. R.; Buchalova, M.; Perkins, C. M.; Alcock, N. W.; Kahol, P. K.; Raghunathan, A.; Busch, D. H. *J. Am. Chem. Soc.* **2000**, *122*, 2512–2522.
(34) Barefield, E. K. *Coord. Chem. Rev.* **2010**, *254*, 1607–1627.
(35) Yin, G.; McCormick, J. M.; Buchalova, M.; Danby, A. M.; Rodgers, K.; Day, V. W.; Smith, K.; Perkins, C. M.; Kitko, D.; Carter, J. D.; Scheper, W. M.; Busch, D. H. *Inorg. Chem.* **2006**, *45*, 8052–8061.
(36) McDonald, A. R.; Bukowski, M. R.; Farquhar, E. R.; Jackson, T. A.; Koehntop, K. D.; Seo, M. S.; De Hont, R. F.; Stubna, A.; Halfen, J. A.; Munck, E.; Nam, W.; Que, L. J. *J. Am. Chem. Soc.* **2010**, *132*, 17118–17129.
(37) Zang, Y.; Kim, J.; Dong, Y.; Wilkinson, E. C.; Appelman, E. H.; Que, L., Jr. *J. Am. Chem. Soc.* **1997**, *119*, 4197–4205.
(38) Chen, K.; Costas, M.; Kim, J.; Tipton, A. K.; Que, L., Jr. *J. Am. Chem. Soc.* **2002**, *124*, 3026–3035.
(39) Fujita, M.; Costas, M.; Que, L., Jr. *J. Am. Chem. Soc.* **2003**, *125*, 9912–9913.
(40) Mas-Balleste, R.; Fujita, M.; Hemmila, C.; Que, L., Jr. *J. Mol. Catal.* **2006**, *251*, 49–53.
(41) Mas-Balleste, R.; Que, L., Jr. *J. Am. Chem. Soc.* **2007**, *129*, 15964–15972.
(42) White, M. C.; Doyle, A. G.; Jacobsen, E. N. *J. Am. Chem. Soc.* **2001**, *123*, 7194–7195.
(43) Company, A.; Feng, Y.; Güell, M.; Ribas, X.; Luis, J. M.; Que, L., Jr.; Costas, M. *Chem.—Eur. J.* **2009**, *15*, 3356–3362.
(44) Bassan, A.; Blomberg, M. R. A.; Siegbahn, P. E. M.; Que, L., Jr. *J. Am. Chem. Soc.* **2002**, *124*, 11056–11063.
(45) Bassan, A.; Blomberg, M. R. A.; Siegbahn, P. E. M.; Que, L., Jr. *Chem.—Eur. J.* **2005**, *11*, 692–705.
(46) Chen, M. S.; White, M. C. *Science* **2007**, *318*, 783–787.
(47) Chen, M. S.; White, M. C. *Science* **2010**, *327*, 566–571.